ACS Photonics

pubs.acs.org/journal/apchd5

Article

Active Graphene Plasmonics with a Drift-Current Bias

Tiago A. Morgado and Mário G. Silveirinha*

Cite This: https://doi.org/10.1021/acsphotonics.0c01890

Read Online

ACCESS | Metrics & More | Article Recommendations | Supporting Information

ABSTRACT: We theoretically demonstrate that a system formed by a drift-current biased graphene sheet on a silicon carbide substrate enables loss compensation and plasmon amplification. The active response of the graphene sheet is rooted in the optical pumping of the graphene plasmons with the gain provided by the streaming current carriers. The proposed system behaves as an optical amplifier for the plasmons copropagating with the drifting electrons and as a strong attenuator for the counter-propagating plasmons. Furthermore, we show that the feedback obtained by connecting the input and output of the system, for example, as a ring-shaped graphene–silicon carbide nanoresonator, combined with the optical gain provided by the drifting electrons, may lead to spasing.

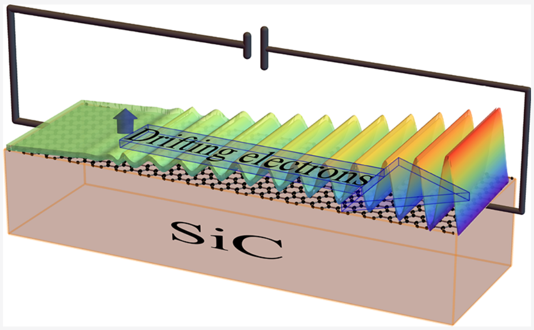

KEYWORDS: *graphene, plasmonics, nonreciprocity, active medium*

■ INTRODUCTION

The unprecedented field enhancement and subwavelength confinement provided by surface plasmon polaritons (SPPs),[1] charge density waves supported by metal-type surfaces, have pushed the field of plasmonics[2−4] to the frontline of scientific research. The unique features of the SPPs opened the door to a plethora of new phenomena and important applications, such as in nanophotonic circuitry,[5,6] photonic metamaterials,[7] solar energy harvesting,[8] superlensing,[9,10] chemical and medical sensing,[11−13] and photothermal cancer therapy.[14,15]

With the isolation of graphene[16] and the discovery of its remarkable electronic and optical properties,[17,18] the field of plasmonics experienced a new boost.[19−24] Much of the interest in graphene plasmonics comes from the fact that the optical properties of this one-atom thick material are highly tunable by means of chemical doping or electrostatic gating, offering a unique opportunity to dynamically manipulate the SPPs properties.

Unfortunately, the high absorption (or ohmic) losses that intrinsically characterize plasmonic materials, such as metals and semiconductors, caused by different scattering mechanisms (e.g., electron−phonon and electron−electron scattering) and by Landau damping[25,26] impose harsh limitations in many nanophotonic applications. For instance, the ohmic losses in silver may limit the SPP propagation length to about 20 nm at near-UV frequencies where the field confinement is strongest.[27] The propagation length increases to values up to 20 μm for visible frequencies but at the expense of poor wave localization.[1,27] The plasmonic dissipation in graphene is also quite significant,[28−31] restricting the SPP propagation length to 1 μm at mid-infrared frequencies and room temperature, and to about 10 μm at cryogenic temperatures.[32]

Even though the development of new plasmonic materials[33−35] may help mitigate the detrimental effects of ohmic losses, the ultimate limits imposed by plasmonic absorption (e.g., in the SPP propagation length or even in the resolution of superlenses) can be only surpassed by introducing optical gain into the systems. In this context, several theoretical and experimental studies on plasmonic loss compensation and SPP amplification have been reported.[27,36−54] In particular, the amplification of long-range SPPs was experimentally demonstrated in systems formed by gold nanofilms combined with optically pumped gain media such as dye solutions[47] and fluorescent polymers.[48] Moreover, merging the SPP amplification with some feedback mechanism may lead to the spontaneous generation of SPPs, an effect known as spasing or plasmonic lasing.[55−65]

In this work, we theoretically predict the full compensation of plasmonic loss and the amplification of SPPs in a nanostructure formed by a drift-current biased graphene sheet deposited on a silicon carbide (SiC) substrate [see Figure 1]. The graphene−SiC plasmons gain energy from the electrons drifting on the graphene sheet, a process known as "negative Landau damping".[66] It is shown that the considered graphene−SiC nanostructure acts as an amplifier for the SPPs copropagating with the drifting electrons and as a very effective attenuator for the counter-propagating plasmons. Moreover,

Received: December 12, 2020

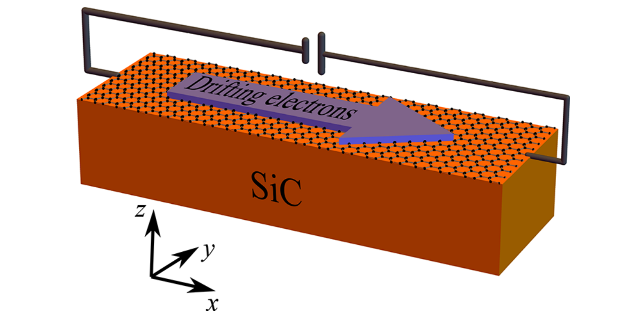

Figure 1. Drift-current biased graphene sheet on a SiC substrate. A graphene sheet deposited on the top of a SiC substrate is biased with a drift-electric current due to a static voltage generator.

we demonstrate that by connecting the input and the output of the system, for example, with a ring-shaped graphene−SiC nanostructure, it may be possible to spontaneously generate graphene SPPs (spasing[55−65]). It should be mentioned that the SPP amplification by means of a drift current biasing was studied in refs 67 and 68 in a related system but with the effect of the drift current bias on the SPP waves treated simply by adapting classical formulas from microwave theory to the graphene.

■ RESULTS AND DISCUSSION

Figure 1 presents a schematic illustration of the structure under study. It consists of a graphene sheet biased with a drift electric current deposited on the top of a SiC substrate. We assume that the region above graphene is air. The frequency dispersion and dissipation in SiC are modeled by the dielectric function reported in refs 24 and 69. As long as $k_B T \ll \mu_c$ (where k_B is the Boltzmann's constant, T is the temperature, and μ_c is the chemical potential), the graphene sheet response (without drifting electrons) may be characterized by the "low-temperature" nonlocal random-phase approximation (RPA) surface conductivity $\sigma_g(\omega, q)$ ($q = \sqrt{k_x^2 + k_y^2}$ is the in-plane wavenumber) reported in ref 21, which includes both the intraband and interband contributions. For ω and q complex, we evaluate $\sigma_g(\omega, q)$ using the analytical continuation formulas reported in ref 70. The loss due to electronic scattering is modeled using the relaxation-time approximation.[71] We assume throughout this article that the relaxation time in graphene is $\tau = 170$ fs,[72,73] which is a conservative value compared to more recent observations.[32] Moreover, in the main text the chemical potential of the graphene sheet is taken equal to $\mu_c = 0.35$ eV. For this chemical potential, the low-temperature limit $k_B T \ll \mu_c$ is satisfied for temperatures up to 400 K. The space-time variation is assumed to be of the form $e^{ik_x x} e^{-i\omega t}$.

The graphene conductivity in the presence of a drift-current bias may be obtained from the conductivity without drift using a Galilean-Doppler shift[66,74]

$$\sigma_g^{\text{drift}}(\omega, k_x) \approx (\omega/\tilde{\omega})\sigma_g(\tilde{\omega}, q)|_{q=\sqrt{k_x^2}} \tag{1}$$

where $\tilde{\omega} = \omega - k_x v_0$ is the Doppler-shifted frequency and k_x is the wavenumber along the x-direction. Here, $\sigma_g(\omega, q)$ is the nonlocal no-drift graphene conductivity discussed in the previous paragraph. It is assumed that the drifting electrons flow along the x-direction with drift velocity v_0 [see Figure 1] and that the in-plane electric field is oriented along x (longitudinal excitation). The drift velocity is typically some fraction of the Fermi velocity v_F. Remarkably, for sufficiently large positive v_0 and k_x, ω and $\tilde{\omega}$ have different signs, and consequently $\text{Re}\{\sigma_g^{\text{drift}}(\omega, k_x)\}$ may become negative in the upper-half frequency plane. Thereby, the drifting electrons may turn the graphene sheet into an active medium with optical gain[66] [see Figure 2]. The impact of collisions (scattering loss) on $\text{Re}\{\sigma_g^{\text{drift}}(\omega, k_x)\}$ is further discussed in the Supporting Information. In Figure 2, $\hbar$ is the reduced Planck constant and $k_F = \mu_c/(\hbar v_F)$ is the Fermi wavenumber.

Before discussing the loss compensation and plasmon amplification in the graphene−SiC waveguide, it is instructive to first examine the scattering properties of the drift-current biased graphene sheet when it is deposited on the top of a dielectric slab. To this end, we consider that a transverse magnetic (TM) wave with magnetic field directed along y [see the inset of Figure 3] and characterized by the wavenumber k_x illuminates the graphene sheet. The complex amplitude of the incident magnetic field is denoted by H_y^{inc} and the (real-valued) oscillation frequency by ω.

Because of the intrinsic material absorption, the superposition of the incident and reflected evanescent waves typically gives rise to a power flux toward the graphene

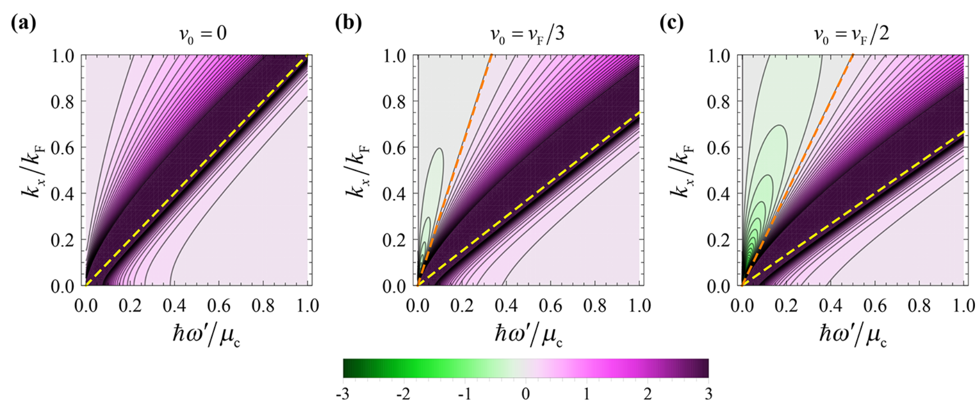

Figure 2. Graphene conductivity. Real part of the graphene conductivity in the upper-half frequency-plane as a function of the normalized frequency $\hbar\omega'/\mu_c$ ($\omega = \omega' + i\omega''$ with $\hbar\omega''/\mu_c = 0.001$) and wavenumber k_x/k_F for different drift velocities v_0. The conductivity normalization factor in the contour plots is $\sigma_0 = e^2/(4\hbar)$, with e the electron charge. The yellow dashed line corresponds to the square-root singularity of the graphene conductivity that occurs at $\omega' \approx k_x'(v_F + v_0)$.[70] The orange dashed lines in (b,c) correspond to $\omega' = k_x' v_0$. The negative Landau damping emerges in the region $\omega' < k_x' v_0$ (region on the left-hand side of the orange line).

https://doi.org/10.1021/acsphotonics.0c01890
ACS Photonics XXXX, XXX, XXX−XXX

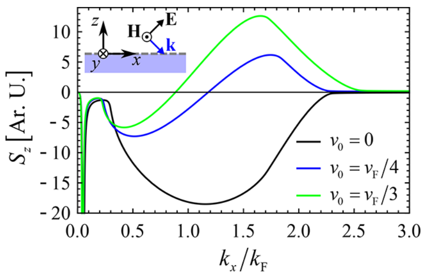

Figure 3. Poynting vector for plane wave incidence. Poynting vector (component perpendicular to the interface in arbitrary units) as a function of k_x for different drift velocities at f = 25 THz. The inset depicts a TM plane wave illuminating the drift-current biased graphene sheet on a dielectric substrate with relative permittivity $\varepsilon_{r,d}$ = 4.

sheet. The z-component of the total Poynting vector in the air region is given by $S_z = \frac{H_y^{inc}}{2\omega\varepsilon_0}\mathrm{Im}\{\gamma_0(1-R)(1+R)^*\}$. Here,

$$R(\omega, k_x) = \frac{\gamma_0\gamma_d + \kappa_g^{drift}(\gamma_d - \gamma_0\varepsilon_{r,d})}{\gamma_0\gamma_d - \kappa_g^{drift}(\gamma_d + \gamma_0\varepsilon_{r,d})} \tag{2}$$

is the magnetic field reflection coefficient,[75] $\kappa_g^{drift} = i\omega\varepsilon_0/\sigma_g^{drift}$, ε_0 is the free-space permittivity, $\gamma_0 = \sqrt{k_x^2 - (\omega/c)^2}$ and $\gamma_d = \sqrt{k_x^2 - \varepsilon_{r,d}(\omega/c)^2}$ are the attenuation constants (along z) in the air and dielectric regions, respectively, c is the speed of light in vacuum, and the "*" symbol denotes complex conjugation. Evidently, in the absence of a drift-current biasing the z-component of the Poynting vector is negative ($S_z < 0$) and thereby the graphene sheet absorbs energy (see the black curve in Figure 3). In contrast, with the drift-current biasing and for a large k_x (blue and green curves in Figure 3), the energy density flux S_z may flip its sign so that the graphene sheet may generate energy that flows away from it. This gain regime stems from the negative Landau damping effect reported in ref 66 which enables the transfer of kinetic energy from the drifting electrons to the radiation field.

To study the opportunities created by the negative Landau damping effect, next we characterize the SPPs supported by the graphene−SiC system illustrated in Figure 1. The dispersion characteristic of the SPPs is given by[24]

$$\frac{1}{\gamma_0} + \frac{\varepsilon_{r,SiC}(\omega)}{\gamma_{SiC}} - \frac{\sigma_g^{drift}}{i\omega\varepsilon_0} = 0 \tag{3}$$

where $\varepsilon_{r,SiC}$ (ω) is the SiC dielectric function[24,69] and $\gamma_{SiC} = \sqrt{k_x^2 - \varepsilon_{r,SiC}(\omega/c)^2}$ is the attenuation constant (along z) of the plasmons in the SiC slab. If the drift velocity is set identical to zero ($\sigma_g^{drift} \to \sigma_g$), one recovers the well-known dispersion equation for the plasmons supported by the graphene−SiC system.

Figure 4 depicts the dispersion characteristic of the SPPs supported by the structure for different drift velocities v_0. The dispersion is found by solving eq 3 with respect to $k_x = k_x' + ik_x''$ for real-valued ω. For low-frequencies, the SiC behaves as a dielectric with positive permittivity. This happens for ω below the SiC resonance frequency $\omega_{TO}/(2\pi)$ = 22.78 THz (ω_{TO} is the bulk transverse optical (TO) phonon frequency).[24,69] In such a regime, the system is analogous to a graphene sheet placed on the top of a dielectric substrate, similar to the systems analyzed by us in refs 70 and 75. As shown in previous works,[70,75−80] the drift-current biasing causes a symmetry

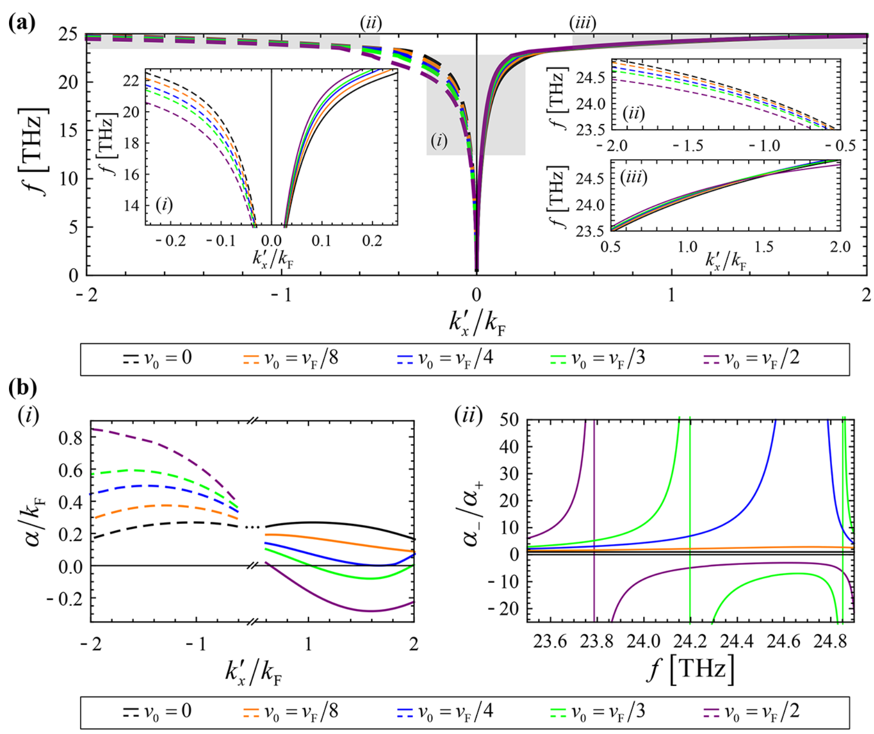

Figure 4. SPPs dispersion diagrams. (a) Main panel: Frequency dispersion of the SPPs supported by the graphene−SiC system as a function of the real part of the SPP wavenumber for several drift velocities v_0; (i), (ii), and (iii) zoom-in views of the shaded rectangular areas of the main panel. (b) (i) SPP attenuation constant ($\alpha = k_x''\,\mathrm{sgn}(k_x')$) as a function of the real part of the SPP wavenumber. (ii) Ratio between the attenuation constants of the SPPs that propagate along the $-x$ and $+x$ direction as a function of the frequency.

https://doi.org/10.1021/acsphotonics.0c01890
ACS Photonics XXXX, XXX, XXX−XXX

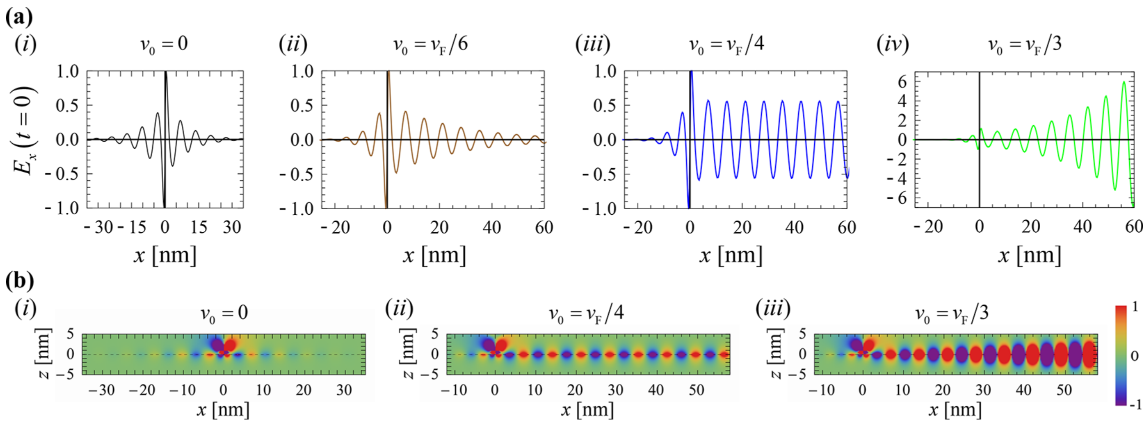

Figure 5. SPP excitation by a near-field emitter. (a) Time snapshots of the x-component of the electric field E_x (in arbitrary unities) as a function of x and for $z = 0$, for several drift velocities v_0. (b) Time snapshots of the x-component of the electric field E_x as a function of x and z and for several drift velocities v_0. The frequency of operation is $\omega/(2\pi) = 24.7$ THz and the emitter is positioned at the point $(x, z) = (0, 1\text{ nm})$. The drift velocity v_0 is indicated at the top of each panel.

breaking in the SPPs dispersion such that $\omega(k_x') \neq \omega(-k_x')$ [see inset (i) of Figure 4a]. Similar nonreciprocal effects may also occur in systems with moving components.[81−83] Clearly, the degree of asymmetry increases with the drift velocity v_0, and for sufficiently large v_0 it gives rise to regimes of unidirectional propagation wherein the SPPs are allowed to propagate only along the $+x$ direction (the direction of the drifting electrons).[70,75]

On the other hand, for frequencies above the resonance and below 27.82 THz, the real part of the SiC permittivity is negative ($\mathrm{Re}\{\varepsilon_{SiC}\} < 0$) and thereby SiC has a plasmonic (metal-type) response.[24,69] In this article, we focus on the spectral range [22.78−27.82 THz] wherein $\mathrm{Re}\{\varepsilon_{SiC}(\omega)\} < 0$. In this range, the system supports plasmons with very short wavelengths, which are essential to access the optical gain regime with $\mathrm{Re}\{\sigma_g^{\mathrm{drift}}\} < 0$ characterized by $\omega - k_x' v_0 < 0$.

The metal-phase of SiC, when $\mathrm{Re}\{\varepsilon_{SiC}\} < 0$, leads to a pronounced spectral asymmetry of the graphene plasmons dispersion such that $\omega(k_x') \neq \omega(-k_x')$ [see Figure 4a, especially the insets (ii) and (iii)]. Even more interesting, Figure 4b(i), (ii) show that with the drift-current bias, the attenuation constant $\alpha = k_x'' \,\mathrm{sgn}(k_x')$ of the SPPs copropagating (counter-propagating) with the drifting electrons is greatly reduced (enhanced). Crucially, for large enough drift velocities v_0, the attenuation constant of the SPPs copropagating with the drifting electrons ($k_x' > 0$) vanishes or even becomes negative. Specifically, Figure 4b(i) shows that the graphene plasmons attenuation can be fully suppressed (that is, $\alpha = 0$) for drift velocities on the order of $v_0 = v_F/4$ [see blue solid curve], and for $v_0 > v_F/4$ it can be even overcompensated (that is, $\alpha < 0$) [see green and purple solid curves]. Therefore, these results indicate that for $v_0 \geq v_F/4$, the graphene−SiC system may be either immune to attenuation or behave as an optical amplifier for the graphene plasmons copropagating with the drifting electrons. In contrast, for counter-propagating plasmons ($k_x' < 0$), α increases with the drift velocity v_0 [see dashed curves in Figure 4b(i)], and hence, the drift current strongly suppresses the counter-propagating plasmons.

The SPP amplification strength and bandwidth increase with the drift velocity v_0. Curiously, the amplification strength $-\alpha$ for $v_0 = v_F/2$ may be comparable or even larger than the attenuation factor α of the SPPs without the drift-current biasing [see purple solid and black curves in Figure 4b(i)]. Furthermore, the attenuation strength along the $-x$ direction for $v_0 = v_F/2$ is about 4 times larger than without a drift current [see purple and black dashed curves in Figure 4b(i)]. On the other hand, Figure 4b(ii) shows that the bandwidth of the SPP amplification regime (range of frequencies where $\alpha_+ < 0$) is about 0.6 THz for $v_0 = v_F/3$ [see green curve], increasing up to around 1.2 THz as the drift velocity approaches $v_0 = v_F/2$ [see purple curve]. Interestingly, it is shown in the Supporting Information that by increasing the chemical potential μ_c of graphene, one can boost the amplification bandwidth and the amplification gain $-\alpha$, and thereby reduce the threshold velocity v_0 at which the attenuation is fully suppressed ($\alpha = 0$). This happens because a larger μ_c implies a larger k_x' (that is, the SPPs are more confined), allowing that $\tilde{\omega}$, and consequently $\mathrm{Re}\{\sigma_g^{\mathrm{drift}}(\omega, k_x)\}$, become negative for lower drift velocities. For $v_0 = v_F/2$, our system enables gain bandwidths of about 5% for $\mu_c = 0.35$ eV, increasing to 6% for $\mu_c = 0.5$ eV (see the Supporting Information).

To further highlight the consequences of the loss compensation and gain regimes in the graphene−SiC system, next we consider the scenario wherein a linearly polarized emitter (a short vertical electric dipole) placed in the vicinity of the graphene sheet is used to excite the graphene plasmons. The radiated and scattered fields are obtained from a Sommerfeld-type integral (an inverse Fourier-Laplace transform in k_x) as described in the Supporting Information. Because of the active response of the system, when $v_0 > 0$ the integral in k_x must be calculated along a line in the lower half k_x-plane parallel to the real-k_x axis. The integration path must be below all poles (for details see the Supporting Information).

Figure 5 shows the time snapshots of the x-component of the electric field for a graphene sheet biased with different drift velocities v_0. As expected, without a drift-current biasing ($v_0 = 0$) the two identical counter-propagating SPPs excited by the near-field emitter are equally attenuated as they propagate along the graphene−SiC interface [see Figures 5a,b(i)]. In such circumstances, the SPP field attenuation is simply determined by the graphene and SiC damping rates. Quite differently, when a drift-current biasing is applied ($v_0 \neq 0$), the plasmons copropagating with the drifting electrons (the $+x$ direction) are significantly less attenuated than the plasmons propagating in the opposite direction (the $-x$ direction) [see Figure 5a(ii)]. In particular, for $v_0 = v_F/4$ the system supports

https://doi.org/10.1021/acsphotonics.0c01890
ACS Photonics XXXX, XXX, XXX−XXX

loss-free plasmons that propagate along the $+x$ direction [see Figure 5a(iii) and Figure 5b(ii)], which is consistent with the attenuation suppression predicted in Figure 4b(i),(ii). Notably, for drift velocities $v_0 > v_F/4$ the plasmons copropagating with the drifting electrons (the $+x$ direction) are amplified, whereas the plasmons propagating along the opposite direction are strongly attenuated [see Figure 5a(iv) and Figure 5b(iii)], as expected from the results of Figure 4b(i),(ii). As previously discussed, the optical gain is due to the conversion of kinetic energy of the drifting electrons into plasmon oscillations.[66] In the Supporting Information, we show that by increasing the chemical potential μ_c, it is possible to reach regimes of lossless propagation and plasmon amplification for drift velocities even lower than $v_F/4$.

So far, it was assumed that the graphene−SiC guide has infinite length in the longitudinal direction (x-direction). Let us now consider finite-length nanostructures. In particular, let us consider a "circular" graphene resonator formed by a ring-shaped graphene ribbon with a drift-current bias placed on the top of a SiC substrate, as sketched in Figure 6a. The modes supported by such a ring-shaped graphene resonator can be found enforcing periodic boundary conditions. Specifically, if the perimeter of the resonator is L then the allowed wave numbers are $k_\varphi = 2\pi n/L$, that is, the wavenumber is necessarily real-valued. Thus, the natural modes of a circular resonator can be found by looking for complex-valued solutions $\omega = \omega(k_\varphi)$ of eq 3 with $k_\varphi = 2\pi n/L$ real-valued. The time variation is $e^{-i\omega t} = e^{-i\omega' t}e^{\omega'' t}$ with $\omega = \omega' + i\omega''$ as the complex resonance frequency of the relevant mode. The system will be unstable if $\omega'' > 0$. Here, we neglect the curvature of the circular resonator, so that $\omega = \omega(k_\varphi)$ may be determined from the modal dispersion [eq 3] of the associated planar geometry. Furthermore, the effect of the finite lateral width of the graphene ribbon is disregarded in our analysis. Using these approximations, we depict in Figure 6b,c the real and imaginary parts of the oscillation frequency (ω) as a function of the normalized k_φ for different drift velocities v_0. Remarkably, Figure 6c shows that for $v_0 > v_F/4$ the nanoring resonator supports oscillations that grow exponentially with time ($\omega'' > 0$). The wave instabilities stem from the feedback that is obtained by connecting the input and output of the optical amplifier. As expected, the growth rate increases as the drift velocity v_0 increases, and for $v_0 = v_F/2$ the growth rate (that is, the magnitude of ω'') can be as high as $\omega'' \approx 1.13 \times 10^{12}$ s^{-1}. The emission rate of the plasmons is determined by ω''. In the example of Figure 6c, before the saturation is reached, the energy in the resonator will grow by a factor of $e \approx 2.7$ every $\frac{1}{2\pi}\left|\frac{\omega'}{2\omega''}\right| \approx 10.8$ periods of oscillation. Therefore, the graphene nanoresonator may be regarded as spaser pumped by drifting electrons.[55−65]

In the Supporting Information, it is shown that the relativistic Doppler-shift model for the graphene conductivity[76−78,84,85] leads to qualitatively similar wave instabilities but with a slightly larger growth rate. In our understanding, the Galilean−Doppler shift theory is the most accurate model when the electron−electron interactions predominate and force the electrons to move with constant velocity v_0.[74] In addition, in the Supporting Information it is shown that the wave instabilities are rooted in the intraband light-matter interactions.

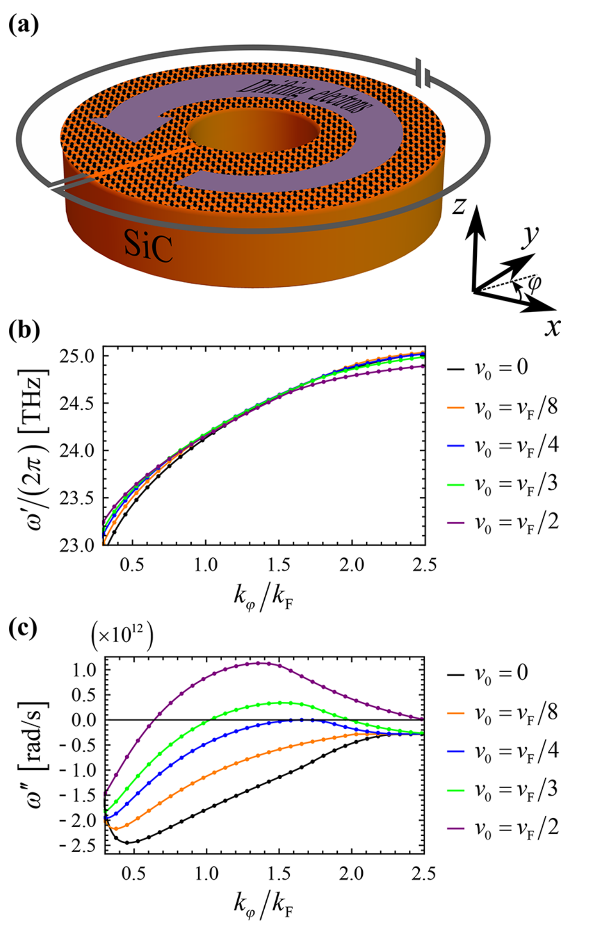

Figure 6. Ring-shaped graphene−SiC nanoresonator. (a) Circular graphene nanoresonator formed by a ring-shaped graphene ribbon biased with a drift current. (b) Real and (c) imaginary parts of the oscillation frequencies of the natural modes as a function of k_φ for different drift velocities v_0. Discrete points: oscillation frequencies for a circular graphene nanoresonator with radius $R = 25$ nm. Solid lines: oscillation frequencies for a circular resonator with $R \to \infty$. The spasing occurs for modes with $\omega'' > 0$.

CONCLUSIONS

In summary, we have demonstrated that a system formed by a drift-current biased graphene sheet deposited on a SiC substrate may enable the full compensation of plasmonic losses and the amplification of graphene plasmons. The plasmonic gain is due to the conversion of the kinetic energy of the moving electrons into short-wavelength plasmons. It was shown that a graphene−SiC waveguide behaves as a one-way optical amplifier. Finally, it was demonstrated that a ring-shaped graphene−SiC resonator can be used as spaser pumped by the drifting electrons.

ASSOCIATED CONTENT

Supporting Information

The Supporting Information is available free of charge at https://pubs.acs.org/doi/10.1021/acsphotonics.0c01890.

(A) The study of the influence of μ_c on the dispersion of the current-driven SPPs and on the SPP field enhancement, (B) derivation of the reflection and transmission coefficients of the graphene−SiC system, (C) derivation of the fields radiated by a linearly polarized emitter placed near the graphene−SiC nanostructure, (D)

https://doi.org/10.1021/acsphotonics.0c01890
ACS Photonics XXXX, XXX, XXX−XXX

comparison of the growth rates predicted by different graphene conductivity models, and (E) the study of the influence of the relaxation time τ on the real part of the drift-current biased graphene conductivity (PDF)

AUTHOR INFORMATION

Corresponding Author

Mário G. Silveirinha − *Instituto Superior Técnico, University of Lisbon, 1049-001 Lisboa, Portugal; Instituto de Telecomunicações, 1049-001 Lisboa, Portugal;* orcid.org/0000-0002-3730-1689; Email: mario.silveirinha@co.it.pt

Author

Tiago A. Morgado − *Instituto de Telecomunicações and Department of Electrical Engineering, University of Coimbra, 3030-290 Coimbra, Portugal;* orcid.org/0000-0002-8500-9885

Complete contact information is available at:
https://pubs.acs.org/10.1021/acsphotonics.0c01890

Notes

The authors declare no competing financial interest.

ACKNOWLEDGMENTS

This work was partially funded by the IET under the A F Harvey Prize, by the Simons Foundation under the award 733700 (Simons Collaboration in Mathematics and Physics, “Harnessing Universal Symmetry Concepts for Extreme Wave Phenomena”), and by Instituto de Telecomunicações (IT) under project UIDB/50008/2020. T.A.M. acknowledges FCT for research financial support with reference CEECIND/04530/2017 under the CEEC Individual 2017 and IT-Coimbra for the contract as an assistant researcher with reference CT/No. 004/2019-F00069.

REFERENCES

(1) Barnes, W. L.; Dereux, A.; Ebbesen, T. W. Surface plasmon subwavelength optics. *Nature* **2003**, *424*, 824−830.

(2) Ozbay, E. Plasmonics: Merging photonics and electronics at nanoscale dimensions. *Science* **2006**, *311*, 189−193.

(3) Gramotnev, D. K.; Bozhevolnyi, S. I. Plasmonics beyond the diffraction limit. *Nat. Photonics* **2010**, *4*, 83−91.

(4) Schuller, J. A.; Barnard, E. S.; Cai, W.; Jun, Y. C.; White, J. S.; Brongersma, M. L. Plasmonics for extreme light concentration and manipulation. *Nat. Mater.* **2010**, *9*, 193−204.

(5) Engheta, N. Circuits with Light at Nanoscales: Optical Nanocircuits inspired by metamaterials. *Science* **2007**, *317*, 1698−1702.

(6) Ebbesen, T. W.; Genet, C.; Bozhevolnyi, S. I. Surface-plasmon circuitry. *Phys. Today* **2008**, *61*, 44−50.

(7) Shalaev, V. M. Optical negative-index metamaterials. *Nat. Photonics* **2007**, *1*, 41−48.

(8) Atwater, H. A.; Polman, A. Plasmonics for improved photovoltaic devices. *Nat. Mater.* **2010**, *9*, 205−213.

(9) Fang, N.; Lee, H.; Sun, C.; Zhang, X. Sub-Diffraction-Limited Optical Imaging with a Silver Superlens. *Science* **2005**, *308*, 534−537.

(10) Kawata, S.; Inouye, Y.; Verma, P. Plasmonics for near-field nano-imaging and superlensing. *Nat. Photonics* **2009**, *3*, 388−394.

(11) Lal, S.; Link, S.; Halas, N. J. Nano-optics from sensing to waveguiding. *Nat. Photonics* **2007**, *1*, 641−648.

(12) Anker, J. N.; Hall, W. P.; Lyandres, O.; Shah, N. C.; Zhao, J.; Van Duyne, R. P. Biosensing with plasmonic nanosensors. *Nat. Mater.* **2008**, *7*, 442−453.

(13) Kabashin, A. V.; Evans, P.; Pastkovsky, S.; Hendren, W.; Wurtz, G. A.; Atkinson, R.; Pollard, R.; Podolskiy, V. A.; Zayats, A. V. Plasmonic nanorod metamaterials for biosensing. *Nat. Mater.* **2009**, *8*, 867−871.

(14) Hirsch, L. R.; Stafford, R. J.; Bankson, J. A.; Sershen, S. R.; Rivera, B.; Price, R. E.; Hazle, J. D.; Halas, N. J.; West, J. L. Nanoshell-mediated near-infrared thermal therapy of tumors under magnetic resonance guidance. *Proc. Natl. Acad. Sci. U. S. A.* **2003**, *100*, 13549−13554.

(15) Lal, S.; Clare, S. E.; Halas, N. J. Nanoshell-Enabled Photothermal Cancer Therapy: Impending Clinical Impact. *Acc. Chem. Res.* **2008**, *41*, 1842−1851.

(16) Novoselov, K. S.; Geim, A. K.; Morozov, S. V.; Jiang, D.; Zhang, Y.; Dubonos, S. V.; Grigorieva, I. V.; Firsov, A. A. Electric Field Effect in Atomically Thin Carbon Films. *Science* **2004**, *306*, 666−669.

(17) Novoselov, K. S.; Geim, A. K.; Morozov, S. V.; Jiang, D.; Katsnelson, M. I.; Grigorieva, I. V.; Dubonos, S. V.; Firsov, A. A. Two-dimensional gas of massless Dirac fermions in graphene. *Nature (London, U. K.)* **2005**, *438*, 197−200.

(18) Geim, A. K.; Novoselov, K. S. The rise of graphene. *Nat. Mater.* **2007**, *6*, 183−191.

(19) Jablan, M.; Buljan, H.; Soljačić, M. Plasmonics in graphene at infrared frequencies. *Phys. Rev. B: Condens. Matter Mater. Phys.* **2009**, *80*, 245435.

(20) Vakil, A.; Engheta, N. Transformation Optics using Graphene. *Science* **2011**, *332*, 1291−1294.

(21) Koppens, F. H. L.; Chang, D. E.; García de Abajo, F. J. Graphene Plasmonics: A Platform for Strong Light−Matter Interactions. *Nano Lett.* **2011**, *11* (8), 3370−3377.

(22) Ju, L.; Geng, B.; Horng, J.; Girit, C.; Martin, M.; Hao, Z.; Bechtel, H. A.; Liang, X.; Zettl, A.; Shen, Y. R.; Wang, F. Graphene plasmonics for tunable terahertz metamaterials. *Nat. Nanotechnol.* **2011**, *6*, 630−634.

(23) Grigorenko, A. N.; Polini, M.; Novoselov, K. S. Graphene Plasmonics. *Nat. Photonics* **2012**, *6*, 749−758.

(24) Gonçalves, P. A. D.; Peres, N. M. R. *An introduction to graphene plasmonics*; World Scientific: Hackensack, NJ, 2016.

(25) Khurgin, J. B. How to deal with the loss in plasmonics and metamaterials. *Nat. Nanotechnol.* **2015**, *10*, 2−6.

(26) Boriskina, S. V.; Cooper, T. A.; Zeng, L.; Ni, G.; Tong, J. K.; Tsurimaki, Y.; Huang, Y.; Meroueh, L.; Mahan, G.; Chen, G. Losses in plasmonics: from mitigating energy dissipation to embracing loss-enabled functionalities. *Adv. Opt. Photonics* **2017**, *9* (4), 775−827.

(27) Berini, P.; De Leon, I. Surface-plasmon-polariton amplifiers and lasers. *Nat. Photonics* **2012**, *6*, 16−24.

(28) Fei, Z.; Rodin, A. S.; Andreev, G. O.; Bao, W.; McLeod, A. S.; Wagner, M.; Zhang, L. M.; Zhao, Z.; Thiemens, M.; Dominguez, G.; Fogler, M. M.; Castro Neto, A. H.; Lau, C. N.; Keilmann, F.; Basov, D. N. Gate-tuning of graphene plasmons revealed by infrared nano-imaging. *Nature* **2012**, *487*, 82−85.

(29) Chen, J.; Badioli, M.; Alonso-González, P.; Thongrattanasiri, S.; Huth, F.; Osmond, J.; Spasenović, M.; Centeno, A.; Pesquera, A.; Godignon, P.; Elorza, A. Z.; Camara, N.; García de Abajo, F. J.; Hillenbrand, R.; Koppens, F. H. L. Optical nano-imaging of gate-tunable graphene plasmons. *Nature* **2012**, *487*, 77−81.

(30) Tassin, P.; Koschny, T.; Kafesaki, M.; Soukoulis, C. M. A comparison of graphene, superconductors and metals as conductors for metamaterials and plasmonics. *Nat. Photonics* **2012**, *6*, 259−264.

(31) Woessner, A.; Lundeberg, M. B.; Gao, Y.; Principi, A.; Alonso-González, P.; Carrega, M.; Watanabe, K.; Taniguchi, T.; Vignale, G.; Polini, M.; Hone, J.; Hillenbrand, R.; Koppens, F. H. L. Highly confined low-loss plasmons in graphene−boron nitride heterostructures. *Nat. Mater.* **2015**, *14*, 421−425.

(32) Ni, G. X.; McLeod, A. S.; Sun, Z.; Wang, L.; Xiong, L.; Post, K. W.; Sunku, S. S.; Jiang, B. Y.; Hone, J.; Dean, C. R.; Fogler, M. M.; Basov, D. N. Fundamental limits to graphene plasmonics. *Nature* **2018**, *557*, 530−533.

(33) West, P. R.; Ishii, S.; Naik, G. V.; Emani, N. K.; Shalaev, V. M.; Boltasseva, A. Searching for better plasmonic materials. *Laser Photonics Rev.* **2010**, *4*, 795−808.

(34) Soukoulis, C. M.; Wegener, M. Optical metamaterials – more bulky and less lossy. *Science* **2010**, *330*, 1633−1634.
(35) Boltasseva, A.; Atwater, H. A. Low-Loss Plasmonic Metamaterials. *Science* **2011**, *331*, 290−291.
(36) Plotz, G.; Simon, H.; Tucciarone, J. Enhanced total reflection with surface plasmons. *J. Opt. Soc. Am.* **1979**, *69*, 419−422.
(37) Sudarkin, A. N.; Demkovich, P. A. Excitation of surface electromagnetic waves on the boundary of a metal with an amplifying medium. *Sov. Phys. Technol. Phys.* **1988**, *34*, 764−766.
(38) Avrutsky, I. Surface plasmons at nanoscale relief gratings between a metal and a dielectric medium with optical gain. *Phys. Rev. B: Condens. Matter Mater. Phys.* **2004**, *70*, 155416.
(39) Nezhad, M. P.; Tetz, K.; Fainman, Y. Gain assisted propagation of surface plasmon polaritons on planar metallic waveguides. *Opt. Express* **2004**, *12*, 4072−4079.
(40) Seidel, J.; Grafstrom, S.; Eng, L. Stimulated emission of surface plasmons at the interface between a silver film and an optically pumped dye solution. *Phys. Rev. Lett.* **2005**, *94*, 177401.
(41) Noginov, M. A.; Zhu, G.; Bahoura, M.; Adegoke, J.; Small, C. E.; Ritzo, B. A.; Drachev, V. P.; Shalaev, V. M. Enhancement of surface plasmons in an Ag aggregate by optical gain in a dielectric medium. *Opt. Express* **2006**, *31*, 3022−3024.
(42) Alam, M. Z.; Meier, J.; Aitchison, J. S.; Mojahedi, M. Gain assisted surface plasmon polariton in quantum wells structures. *Opt. Express* **2007**, *15*, 176−182.
(43) Genov, D. A.; Ambati, M.; Zhang, X. Surface plasmon amplification in planar metal films. *IEEE J. Quantum Electron.* **2007**, *43*, 1104−1108.
(44) Noginov, M. A.; Podolskiy, V. A.; Zhu, G.; Mayy, M.; Bahoura, M.; Adegoke, J. A.; Ritzo, B. A.; Reynolds, K. Compensation of loss in propagating surface plasmon polariton by gain in adjacent dielectric medium. *Opt. Express* **2008**, *16*, 1385−1392.
(45) De Leon, I.; Berini, P. Theory of surface plasmon-polariton amplification in planar structures incorporating dipolar gain media. *Phys. Rev. B: Condens. Matter Mater. Phys.* **2008**, *78*, 161401.
(46) Bolger, P. M.; Dickson, W.; Krasavin, A. V.; Liebscher, L.; Hickey, S. G.; Skryabin, D. V.; Zayats, A. V. Amplified spontaneous emission of surface plasmon polaritons and limitations on the increase of their propagation length. *Opt. Lett.* **2010**, *35*, 1197−1199.
(47) De Leon, I.; Berini, P. Amplification of long-range surface plasmons by a dipolar gain medium. *Nat. Photonics* **2010**, *4*, 382−387.
(48) Gather, M. C.; Meerholz, K.; Danz, N.; Leosson, K. Net optical gain in a plasmonic waveguide embedded in a fluorescent polymer. *Nat. Photonics* **2010**, *4*, 457−461.
(49) Fedyanin, D. Y.; Krasavin, A. V.; Arsenin, A. V.; Zayats, A. V. Surface Plasmon Polariton Amplification upon Electrical Injection in Highly Integrated Plasmonic Circuits. *Nano Lett.* **2012**, *12* (5), 2459−2463.
(50) Liu, N.; Wei, H.; Li, J.; Wang, Z.; Tian, X.; Pan, A.; Xu, H. Plasmonic Amplification with Ultra-High Optical Gain at Room Temperature. *Sci. Rep.* **2013**, *3*, 1967.
(51) Kéna-Cohen, S.; Stavrinou, P. N.; Bradley, D. D.; Maier, S. A. Confined Surface Plasmon-Polariton Amplifiers. *Nano Lett.* **2013**, *13* (5), 1323−1329.
(52) Xiao, S.; Drachev, V. P.; Kildishev, A. V.; Ni, X.; Chettiar, U.; Yuan, H. K.; Shalaev, V. M. Loss-free and active optical negative-index metamaterials. *Nature* **2010**, *466*, 735−738.
(53) Hess, O.; Pendry, J. B.; Maier, S. A.; Oulton, R. F.; Hamm, J. M.; Tsakmakidis, K. L. Active nanoplasmonic metamaterials. *Nat. Mater.* **2012**, *11*, 573−584.
(54) Galiffi, E. E.; Huidobro, P. A.; Pendry, J. B. Broadband Nonreciprocal Amplification in Luminal Metamaterials. *Phys. Rev. Lett.* **2019**, *123*, 206101.
(55) Bergman, D. J.; Stockman, M. I. Surface Plasmon Amplification by Stimulated Emission of Radiation: Quantum Generation of Coherent Surface Plasmons in Nanosystems. *Phys. Rev. Lett.* **2003**, *90*, 027402.
(56) Hill, M. T.; Oei, Y.-S.; Smalbrugge, B.; Zhu, Y.; de Vries, T.; van Veldhoven, P. J.; van Otten, F. W. M.; Eijkemans, T. J.; Turkiewicz, J. P.; de Waardt, H.; Geluk, E. J.; Kwon, S.-H.; Lee, Y.-H.; Nötzel, R.; Smit, M. K. Lasing in metallic-coated nanocavities. *Nat. Photonics* **2007**, *1*, 589−594.
(57) Zheludev, N. I.; Prosvirnin, S. L.; Papasimakis, N.; Fedotov, V. A. Lasing Spaser. *Nat. Photonics* **2008**, *2*, 351−354.
(58) Noginov, M. A.; Zhu, G.; Belgrave, A. M.; Bakker, R.; Shalaev, V. M.; Narimanov, E. E.; Stout, S.; Herz, E.; Suteewong, T.; Wiesner, U. Demonstration of a spaser-based nanolaser. *Nature (London, U. K.)* **2009**, *460*, 1110−1112.
(59) Oulton, R. F.; Sorger, V. J.; Zentgraf, T.; Ma, R.-M.; Gladden, C.; Dai, L.; Bartal, G.; Zhang, X. Plasmon lasers at deep subwavelength scale. *Nature (London, U. K.)* **2009**, *461*, 629−632.
(60) Hill, M. T.; Marell, M.; Leong, E. S. P.; Smalbrugge, B.; Zhu, Y.; Sun, M.; van Veldhoven, P. J.; Geluk, E. J.; Karouta, F.; Oei, Y.-S.; Nötzel, R.; Ning, C.-Z.; Smit, M. K. Lasing in metal-insulator-metal sub-wavelength plasmonic waveguides. *Opt. Express* **2009**, *17*, 11107.
(61) Nezhad, M.; Simic, A.; Bondarenko, O.; Slutsky, B.; Mizrahi, A.; Feng, L.; Lomakin, V.; Fainman, Y. Room-temperature subwavelength metallo-dielectric lasers. *Nat. Photonics* **2010**, *4*, 395−399.
(62) Kwon, S.-H.; Kang, J.-H.; Seassal, C.; Kim, S.-K.; Regreny, P.; Lee, Y.-H.; Lieber, C. M.; Park, H.-G. Subwavelength Plasmonic Lasing from a Semiconductor Nanodisk with Silver Nanopan Cavity. *Nano Lett.* **2010**, *10*, 3679−3683.
(63) Ma, R. M.; Oulton, R. F.; Sorger, V. J.; Bartal, G.; Zhang, X. Room-temperature sub-diffraction-limited plasmon laser by total internal reflection. *Nat. Mater.* **2011**, *10*, 110−113.
(64) Sorger, V. J.; Zhang, X. Spotlight on Plasmon Lasers. *Science* **2011**, *333*, 709−710.
(65) Oulton, R. F. Surface plasmon lasers: sources of nanoscopic light. *Mater. Today* **2012**, *15*, 26−34.
(66) Morgado, T. A.; Silveirinha, M. G. Negative Landau damping in bilayer graphene. *Phys. Rev. Lett.* **2017**, *119*, 133901.
(67) Dadoenkova, Y. S.; Moiseev, S. G.; Abramov, A. S.; Kadochkin, A. S.; Fotiadi, A. A.; Zolotovskii, I. O. Surface plasmon polariton amplification in semiconductor−graphene−dielectric structure. *Ann. Phys.* **2017**, *529* (5), 1700037.
(68) Zolotovskii, I. O.; Dadoenkova, Y. S.; Moiseev, S. G.; Kadochkin, A. S.; Svetukhin, V. V.; Fotiadi, A. A. Plasmon-polariton distributed-feedback laser pumped by a fast drift current in graphene. *Phys. Rev. A: At., Mol., Opt. Phys.* **2018**, *97*, 053828.
(69) Koch, R. J.; Seyller, Th.; Schaefer, J. A. Strong phonon-plasmon coupled modes in the graphene/silicon carbide heterosystem. *Phys. Rev. B* **2010**, *82*, 201413.
(70) Morgado, T. A.; Silveirinha, M. G. Nonlocal effects and enhanced nonreciprocity in current-driven graphene systems. *Phys. Rev. B: Condens. Matter Mater. Phys.* **2020**, *102*, 075102.
(71) Mermin, N. D. Lindhard dielectric function in the relaxation-time approximation. *Phys. Rev. B* **1970**, *1*, 2362.
(72) Efetov, D. K.; Kim, P. Controlling Electron-Phonon Interactions in Graphene at Ultrahigh Carrier Densities. *Phys. Rev. Lett.* **2010**, *105*, 256805.
(73) Tassin, P.; Koschny, T.; Soukoulis, C. M. Graphene for Terahertz Applications. *Science* **2013**, *341*, 620−621.
(74) Morgado, T. A.; Silveirinha, M. G. Reply to Comment on Negative Landau damping in bilayer graphene. *Phys. Rev. Lett.* **2019**, *123*, 219402.
(75) Morgado, T. A.; Silveirinha, M. G. Drift-induced Unidirectional Graphene Plasmons. *ACS Photonics* **2018**, *5* (11), 4253−4258.
(76) Borgnia, D. S.; Phan, T. V.; Levitov, L. S. Quasi-Relativistic Doppler Effect and Non-Reciprocal Plasmons in Graphene. arXiv:1512.09044, 2015. https://arxiv.org/abs/1512.09044v1.
(77) Van Duppen, B.; Tomadin, A.; Grigorenko, A. N.; Polini, M. Current-induced birefringent absorption and non-reciprocal plasmons in graphene. *2D Mater.* **2016**, *3*, 015011.
(78) Wenger, T.; Viola, G.; Kinaret, J.; Fogelström, M.; Tassin, P. Current-controlled light scattering and asymmetric plasmon propagation in graphene. *Phys. Rev. B: Condens. Matter Mater. Phys.* **2018**, *97*, 085419.

(79) Correas-Serrano, D.; Gomez-Diaz, J. S. Nonreciprocal and collimated surface plasmons in drift-biased graphene. *Phys. Rev. B* **2019**, *100*, 081410.
(80) Prudêncio, F. R.; Silveirinha, M. G. Asymmetric Electron Energy Loss in Drift-Current Biased Graphene. *Plasmonics* **2021**, *16*, 19−26.
(81) Fleury, R.; Sounas, D. L.; Sieck, C. F.; Haberman, M. R.; Alù, A. Sound Isolation and Giant Linear Nonreciprocity in a Compact Acoustic Circulator. *Science* **2014**, *343*, 516−519.
(82) Lannebère, S.; Silveirinha, M. G. Wave instabilities and unidirectional light flow in a cavity with rotating walls. *Phys. Rev. A: At., Mol., Opt. Phys.* **2016**, *94*, 033810.
(83) Mazor, Y.; Alù, A. Nonreciprocal hyperbolic propagation over moving metasurfaces. *Phys. Rev. B: Condens. Matter Mater. Phys.* **2019**, *99*, 045407.
(84) Sabbaghi, M.; Lee, H.-W.; Stauber, T.; Kim, K. S. Drift-induced modifications to the dynamical polarization of graphene. *Phys. Rev. B: Condens. Matter Mater. Phys.* **2015**, *92*, 195429.
(85) Svintsov, D. Emission of plasmons by drifting Dirac electrons: A hallmark of hydrodynamic transport. *Phys. Rev. B: Condens. Matter Mater. Phys.* **2019**, *100*, 195428.

https://doi.org/10.1021/acsphotonics.0c01890
ACS Photonics XXXX, XXX, XXX−XXX